Original Article | Gastrointestinal Imaging

https://doi.org/10.3348/kjr.2017.18.2.289
pISSN 1229-6929 · eISSN 2005-8330
Korean J Radiol 2017;18(2):289-298

Korean Journal of Radiology
KJR

The Effects of Breathing Motion on DCE-MRI Images: Phantom Studies Simulating Respiratory Motion to Compare CAIPIRINHA-VIBE, Radial-VIBE, and Conventional VIBE

Chang Kyung Lee, PhD[1*], Nieun Seo, MD, PhD[1, 2*], Bohyun Kim, MD, PhD[1, 3], Jimi Huh, MD[1, 4], Jeong Kon Kim, MD, PhD[1], Seung Soo Lee, MD, PhD[1], In Seong Kim, MS[5], Dominik Nickel, PhD[6], Kyung Won Kim, MD, PhD[1]

[1]Department of Radiology and Research Institute of Radiology, Asan Medical Center, University of Ulsan College of Medicine, Seoul 05505, Korea; [2]Department of Radiology, Yonsei University College of Medicine, Severance Hospital, Seoul 03722, Korea; [3]Department of Radiology, Ajou Unversity School of Medicine, Suwon 16499, Korea; [4]Department of Radiology, Ulsan University Hospital, Ulsan 44033, Korea; [5]Siemens Healthcare Korea, Seoul 03737, Korea; [6]MR Application Predevelopment, Siemens Healthcare, Erlangen 91052, Germany

Objective: To compare the breathing effects on dynamic contrast-enhanced (DCE)-MRI between controlled aliasing in parallel imaging results in higher acceleration (CAIPIRINHA)-volumetric interpolated breath-hold examination (VIBE), radial VIBE with k-space-weighted image contrast view-sharing (radial-VIBE), and conventional VIBE (c-VIBE) sequences using a dedicated phantom experiment.

Materials and Methods: We developed a moving platform to simulate breathing motion. We conducted dynamic scanning on a 3T machine (MAGNETOM Skyra, Siemens Healthcare) using CAIPIRINHA-VIBE, radial-VIBE, and c-VIBE for six minutes per sequence. We acquired MRI images of the phantom in both static and moving modes, and we also obtained motion-corrected images for the motion mode. We compared the signal stability and signal-to-noise ratio (SNR) of each sequence according to motion state and used the coefficients of variation (CoV) to determine the degree of signal stability.

Results: With motion, CAIPIRINHA-VIBE showed the best image quality, and the motion correction aligned the images very well. The CoV (%) of CAIPIRINHA-VIBE in the moving mode (18.65) decreased significantly after the motion correction (2.56) ($p < 0.001$). In contrast, c-VIBE showed severe breathing motion artifacts that did not improve after motion correction. For radial-VIBE, the position of the phantom in the images did not change during motion, but streak artifacts significantly degraded image quality, also after motion correction. In addition, SNR increased in both CAIPIRINHA-VIBE (from 3.37 to 9.41, $p < 0.001$) and radial-VIBE (from 4.3 to 4.96, $p < 0.001$) after motion correction.

Conclusion: CAIPIRINHA-VIBE performed best for free-breathing DCE-MRI after motion correction, with excellent image quality.

Keywords: *Dynamic contrast-enhanced; Magnetic resonance imaging; Phantom study; Free-breathing; Respiratory motion; Parallel imaging technique; CAIPIRINHA-VIBE*

Received March 15, 2016; accepted after revision October 18, 2016.
This research was supported by a grant of the Bracco Korea (No. 2014-0060) and a grant of the National Research Foundation of Korea funded by the Ministry of Science, ICT & Future Planning (No. 2014R1A1A1006823).
*These authors contributed equally to this work.
Corresponding author: Kyung Won Kim, MD, PhD, Department of Radiology and Research Institute of Radiology, Asan Medical Center, University of Ulsan College of Medicine, 88 Olympic-ro 43-gil, Songpa-gu, Seoul 05505, Korea.
• Tel: (822) 3010-4400 • Fax: (822) 476-4719 • E-mail: kyungwon_kim@amc.seoul.kr

INTRODUCTION

Dynamic contrast-enhanced (DCE)-magnetic resonance imaging (MRI) is a quantitative functional MRI technique that provides information about tumor vascularity and perfusion, which can be used as pharmacodynamic and surrogate outcome biomarkers in cancer patients who are being treated with anti-vascular agents (1).

The vast majority of DCE-MRI in oncologic clinical trials and practice is aimed at assessing tumors in the torso. With DCE-MRI, patients are scanned continuously for several minutes while being allowed to breathe shallowly (1). However, the image quality of free-breathing DCE-MRI of the torso is greatly impaired by respiratory motion artifacts when using conventional three-dimensional (3D) gradient-echo (GRE) T1-weighted imaging (T1-WI) sequences, such as volumetric interpolated breath hold examination (VIBE) (2).

To overcome these respiratory motion artifacts, motion-resistant image acquisition schemes have been developed including radial 3D GRE T1-WI acquisition, radial-VIBE, and controlled aliasing in parallel imaging results in higher acceleration-VIBE (CAIPIRINHA-VIBE) (2-5). When radial VIBE is combined with k-space-weighted image contrast reconstruction (KWIC)–known as radial VIBE with KWIC view-sharing and hereinafter referred to as radial-VIBE–it can generate time-resolved sub-frame images that enable DCE-MRI with high temporal resolution. Radial acquisition schemes are less motion-sensitive than conventional VIBE (c-VIBE), enabling free-breathing MRI examinations (2). CAIPIRINHA-VIBE uses a modified parallel acquisition technique (PAT), which lessens respiratory motion artifacts in particular by reducing scan time (6-8).

However, to our knowledge, no study has evaluated the effects of breathing motion on the DCE-MRI images acquired from these sequences. Therefore, we aimed at conducting a phantom study using a respiratory-motion-simulating platform to compare motion effects on DCE-MRI images among CAIPIRINHA-VIBE, radial-VIBE, and c-VIBE sequences. We assessed the effects of free breathing in terms of the efficacy of motion correction, motion-related artifacts, signal stability, and signal-to-noise ratio (SNR).

MATERIALS AND METHODS

We did not require approval from any kind of Ethical Committee because this was a phantom study. Two authors who are employees of Siemens Healthcare provided technical advice for MRI acquisition but did not participate in the data analysis or interpretation.

Phantom Construction

We modified a standardized quantitative imaging biomarkers alliance (QIBA) DCE-MRI phantom version 2 (9); the detailed information of this phantom is described in a prior study (3). Briefly, this phantom is composed of two rings of tubes containing 50 mL of $NiCl_2$ solutions with different concentrations.

Moving Platform Construction

To simulate the breathing movement, we built a moving platform that consisted of a phantom holder with wheels, a plastic cover box, a handle, and a rail (Fig. 1). During MRI scanning, the DCE-MRI phantom was placed on the phantom holder with wheels, which was movable along the rail, which simulates the movement of internal organs according to respiratory motion; the handle was connected to the moving phantom holder. We cut shallow furrows in the handle at every 1 cm so that the researcher could consistently move the platform at a constant speed of 1 cm/sec. The plastic cover box was fixed, and the MR body coil was placed on top of the cover box.

MRI Acquisition

Using a 3T MR scanner (MAGNETOM Skyra; Siemens Healthcare, Erlangen, Germany) with standard body and spine coil arrays, we acquired the MRIs using CAIPIRINHA-VIBE, a prototypical radial-VIBE, and c-VIBE sequences in both moving and static modes. We obtained repeated series of each sequence over six minutes with a temporal resolution of five seconds, for a total of 72 time points. If we had shortened the temporal resolution of the DCE-MRI, we could have obtained more time points, but we suspected that temporal resolution of 5 seconds could be sufficient to reflect the first pass after the contrast agent injection and to meet the QIBA recommendation (9). The detailed MRI parameters are summarized in Table 1.

For the CAIPIRINHA-VIBE sequence, we used an acceleration factor of four (two in the phase-encoding direction and two in the partition-encoding direction) with a reordering delta shift of 1. Radial-VIBE uses a "stack-of-stars" trajectory, i.e., k-space data are acquired using radial sampling in the in-plane directions and Cartesian phase encoding along the through-plane direction (10-12). During the radial-VIBE image acquisition, the full-frame data were

Korean Journal of Radiology
KJR

obtained over 30.6 seconds with a view-interleaved radial acquisition scheme, specifically angle-bisection reordering, and KWIC reconstruction (13) was applied in order to generate six time-resolved, sub-frame images of 5.1-seconds temporal resolution; we used the time-resolved sub-frame images only for the radial-VIBE image analysis.

We scanned the phantom in a moving mode to simulate breathing motion using CAIPIRINHA-VIBE, radial-VIBE, and c-VIBE. Specifically, a well-trained researcher went into the MR examination room and manually moved the handle that was connected with the phantom holder; to minimize variability due to manual motion, an alarm clock was set to beep every second. The researcher repeatedly moved the platform, superiorly for 3 seconds and inferiorly for 3 seconds at a rate of 1 cm/sec to simulate breathing motion with a respiratory cycle of 6 seconds. Thereafter, the phantom was scanned statically using CAIPIRINHA-VIBE, radial-VIBE, and c-VIBE in order to obtain standard

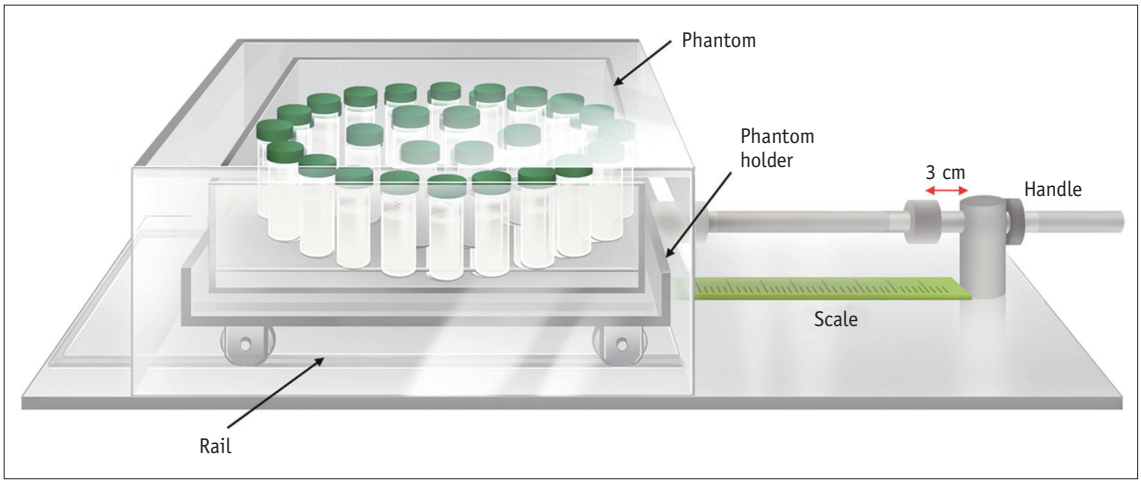

Fig. 1. Schematic figure of DCE-MRI phantom and moving platform. Moving platform consists of phantom holder with wheels, plastic cover box, handle, and rail; MR body coil (not illustrated) was placed on top of cover box. Well-trained researcher manually moved moving platform. DCE-MRI = dynamic contrast-enhanced-magnetic resonance imaging

Table 1. MR Parameters for Dynamic Scanning

Sequences	CAIPIRINHA-VIBE	Radial-VIBE	Conventional VIBE
Orientation	Coronal	Coronal	Coronal
Repetition time/echo time (ms)	3.41/1.11	4.0/1.38	3.74/1.4
Field of view			
Read (mm)	420	420	420
Phase (%)	100	100	100
Matrix			
Base resolution	256	256	256
Phase resolution (%)	100	NA	100
Slice resolution (%)	53	53	53
Slab	1	1	1
Slices per slab	20	20	20
Slice thickness (mm)	4	4	4
Flip angle (°)	25	25	25
No. of excitations	1	1	1
KWIC reconstruction	NA	Yes (6 sub-frames)	NA
Acquisition time (1 series/72 series)	5.1 sec/370 sec	5.1 sec/370 sec	5.0 sec/362 sec
PAT mode	CAIPIRINHA	None	GRAPPA
Acceleration factor	2 × 2	None	2

CAIPIRINHA = controlled aliasing in parallel imaging results in higher acceleration, GRAPPA = generalized auto-calibrating partially parallel acquisition, KWIC = k-space-weighted image contrast, NA = not applicable, PAT = parallel acquisition technique, VIBE = volumetric interpolated breath-hold examination

references to compare with images in a moving mode.

Image Analysis

Image Data Sets

From the DCE-MRI images obtained in a moving mode, we generated motion-corrected images using a dedicated software (Tissue 4D; Siemens Healthcare, Erlangen, Germany). We conducted motion correction with a non-rigid registration technique that aligned the dynamic data set to a defined reference volume by transforming each individual pixel so that the image pixels were displayed in the same geometrical position for both data sets. The advantage of the non-rigid registration is that local changes caused by for example, breathing, can be mapped correctly without having to correct organ or bone positions that are not affected by the local motion (14). Consequently, we could acquire three image sets (i.e., static images, moving images, and motion-corrected images) of each sequence (CAIPIRINHA-VIBE, Radial-VIBE, and c-VIBE) and use them for data analysis.

The Effects of Breathing Motion on the DCE-MRI Images

We visually assessed the effects of breathing motion on the three image sets (static, moving, and motion-corrected) of each sequence (CAIPIRINHA-VIBE, radial-VIBE, and c-VIBE). In particular, we evaluated the motions and shapes of the tubes in the phantom, as well as motion-related artifacts, and compared them between the three image sets.

Signal Stability

To evaluate how much the signal intensity of a subject varied over a DCE-MRI acquisition time (i.e., six minutes), we placed a circular region of interest (ROI) in the tube with the most concentrated $NiCl_2$ solution for each image set of the three sequences and recorded the signal intensities of the ROIs at 72 time points over 6 minutes. We then plotted the measured signal intensities over time (hereafter referred to as time-intensity plots). For the quantitative assessment of the signal stability, we calculated the means and standard deviations (SDs) of the signal intensity from the 72 time points in each sequence. We then derived the coefficients of variation (CoVs) of the signal intensity by dividing the SDs by the means. The CoV (%) is a standardized measure of the dispersion of a distribution, and a small CoV indicates better signal stability (15).

Signal-to-Noise Ratio

We calculated SNR using a method based on a single image voxel (16-18). In MRI images acquired using radial-VIBE or parallel imaging, such as CAIPIRINHA-VIBE, in which noise distribution can be inhomogeneous, SNR based on a single image voxel is known to be more accurate than conventional SNR based on two separate image voxels, i.e., one in the tissue and one in the background to measure the signal intensity and the noise, respectively. In this method based on a single image voxel, SNR is derived from the ratio of the mean and the SD of the signal intensity in repeated "identical acquisitions" over time (16). According to this method, the ROI was drawn at the tube that held the $NiCl_2$ solution with the highest concentration along 72 sequential time points of MR images to measure the means and SDs of single image voxels for each time point.

Statistical Analysis

We compared the signal intensity, SD, and SNR according to motion mode within a sequence using a one-way repeated-measure ANOVA with a post hoc *t* test with Bonferroni correction. We compared the CoVs (%) according to motion mode within a sequence using Levene's test. We performed all statistical analyses using SPSS version 21.0 (IBM Corp., Armonk, NY, USA). *p* values less than 0.05 were considered statistically significant.

RESULTS

The Effects of Breathing Motion on DCE-MRI Images

Videos of the dynamic scanning using CAIPIRINHA-VIBE, radial-VIBE, and c-VIBE in static, moving, and motion-corrected moving modes are presented in the supplementary material. We believe these Supplementary Movie 1 (in the online-only Data Supplement) to be the most important data to obtain an overall intuitive sense of all image sets for the three sequences.

Figure 2 displays the captured images of dynamic scanning using CAIPIRINHA-VIBE, radial-VIBE, and c-VIBE in static, moving, and motion-corrected moving modes, which were aligned according to time (Fig. 2). Static images acquired using all three sequences showed a stable location of the phantom without substantial artifacts. Moving images and motion-corrected images showed the unique characteristics of each sequence.

For the CAIPIRINHA-VIBE, images of moving mode without motion correction demonstrated the up-and-

Korean Journal of Radiology
KJR

down movement of the phantom; notably, the shape of the tubes was maintained during the up-and-down movement, although the overall shape of each tube was mildly distorted. After motion correction, the vertical motion of the phantom was resolved as if motion correction works as rigid registration. In addition, the tubes maintained their shapes without significant distortion. For the radial-VIBE, neither moving nor motion-corrected images displayed significant motion of the phantom, indicating the motion-insensitivity of this sequence. However, the round shape of

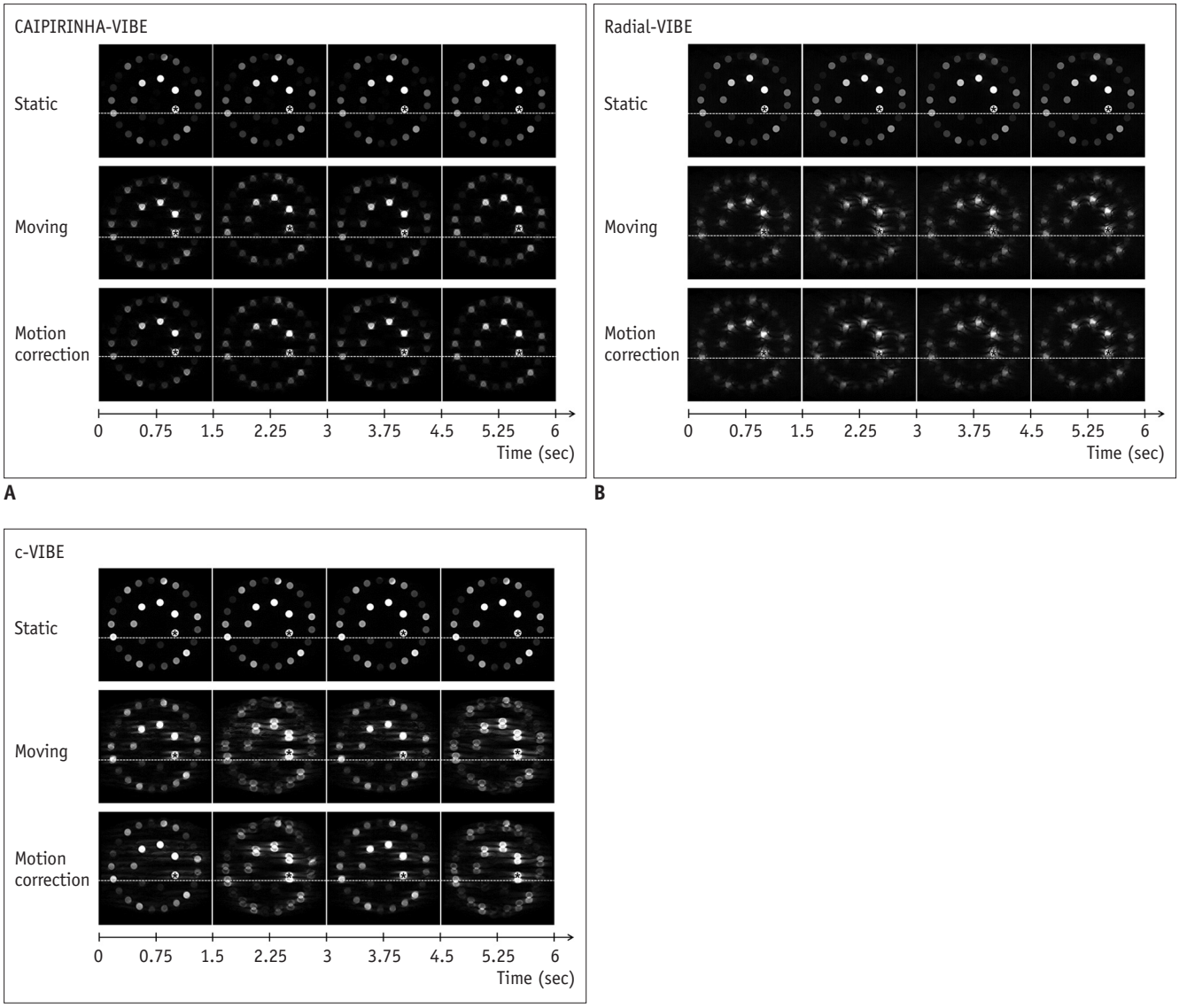

Fig. 2. Captured MRI images of dynamic scanning using each sequence according to motion mode. Each four-image set was arranged in horizontal axis along time points (6 seconds, 1 respiratory cycle in this study). We drew white dotted line below tube (asterisks) that contained highest concentrations of $NiCl_2$ to clearly demonstrate movement.
A. MRI images using CAIPIRINHA-VIBE. For static mode (upper row), phantom showed stable location without any artifact. For moving mode (middle row), MR images obtained using CAIPIRINHA-VIBE showed vertical phantom displacement with mildly distorted tube shapes. After motion correction (lower row), phantom displacement had decreased markedly, with remaining ghosting artifacts around each tube. **B.** MRI images using radial-VIBE. For static mode (upper row), phantom also showed stable location without any artifact. For both moving (middle row) and motion-corrected (lower row) modes, MR images did not show significant displacement of phantom. However, round shape of each tube was significantly distorted due to streak artifacts on radial-VIBE, and these streak artifacts did not grossly improve after motion correction. **C.** MRI images using c-VIBE. For static mode (upper row), phantom also showed stable location without any artifact. For moving mode (middle row), MR images obtained using c-VIBE showed vertical phantom motion with related artifacts; true image of each tube overlapped with after-image of each tube, which disrupted original round shape. Neither displacement due to motion nor motion-related artifacts significantly improved after motion correction (lower row). c-VIBE = conventional VIBE, CAIPIRINHA = controlled aliasing in parallel imaging results in higher acceleration, VIBE = volumetric interpolated breath-hold examination

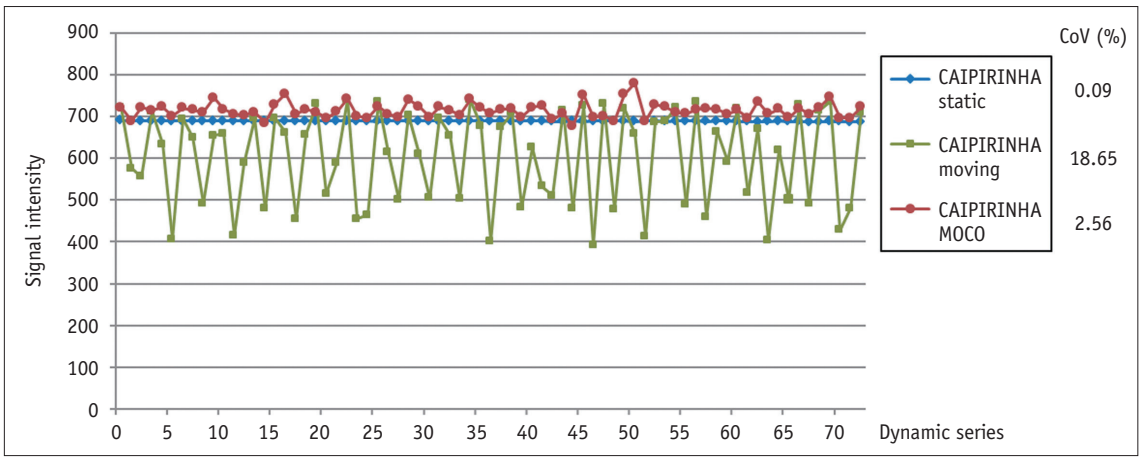

A

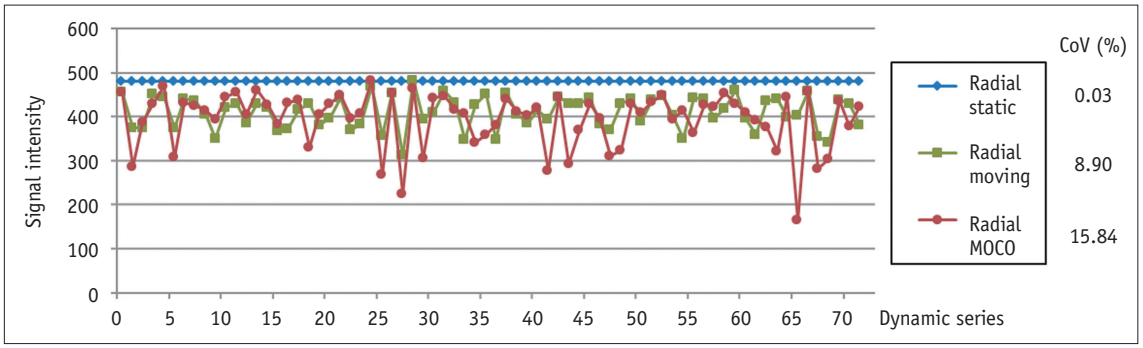

B

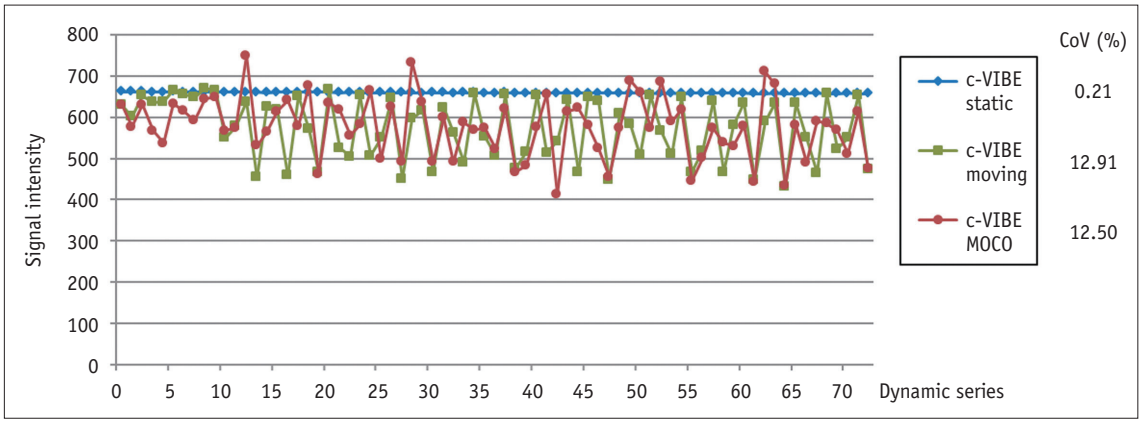

C

Fig. 3. Graphs and CoV (%) for signal stability of each MRI sequence. Signal intensities, which were obtained using each sequence, are plotted along dynamic series over six minutes. Each colored line indicates signal intensities according to motion mode, i.e., blue line, static mode; green line, moving mode; red line, motion-corrected mode. For all three sequences, signal intensities at static mode (blue lines) were stable without variation. Small CoVs, which are close to 0, indicate that variations in MRI signal intensities were negligible, thus suggesting better signal stability.
A. CAIPIRINHA-VIBE. Signal intensities for moving mode (green line) showed periodical vertical fluctuations. In motion-corrected mode (red line), variations in signal intensities observed in moving mode had decreased greatly. CoVs in static, moving, and motion-corrected modes were 0.09, 18.65, and 2.56, respectively. **B.** Radial-VIBE. Variations in signal intensities in radial-VIBE in moving mode (green line) were less prominent than those in CAIPIRINHA-VIBE or c-VIBE; however, these variations in signal intensities did not decrease after motion correction (red line). CoVs for static, moving, and motion-corrected modes were 0.03, 8.90, and 15.84, respectively. **C.** c-VIBE. Signal intensities in moving mode (green line) fluctuated up and down over time, and with motion correction (red line), variations in signal intensities observed in moving mode did not significantly decrease. CoVs in static, moving, and motion-corrected modes were 0.21, 12.91, and 12.50, respectively. c-VIBE = conventional VIBE, CAIPIRINHA = controlled aliasing in parallel imaging results in higher acceleration, CoV = coefficients of variation, MOCO = motion correction, VIBE = volumetric interpolated breath-hold examination

Korean Journal of Radiology
KJR

each tube was degraded due to streak artifacts derived from the radial acquisition scheme, and these streak artifacts did not improve after motion correction. Regarding the c-VIBE, the moving images without motion correction showed phantom motion with significant related blurring, which substantially disrupted the original round shape of the tubes. Motion correction could not adjust for the vertical motion or the related blurring of the phantom.

Signal Stability

The time-intensity plots of the three image sets we obtained from the three sequences and CoVs (%) of the signal intensities are presented in Figure 3. The means and SDs of the signal intensities of all image sets are presented in Table 2. Static image sets of all three sequences showed stable signal intensity over 6 minutes (Fig. 3, blue lines), with a very low CoV (0.09% in CAIPIRINHA-VIBE, 0.03% in radial-VIBE, and 0.21% in c-VIBE). These CoVs were close to 0, indicating that the variation in MRI signal intensities for the static mode was negligible in all sequences. In contrast, moving and motion-corrected image sets showed unique patterns of signal intensity plots according to the characteristics of each sequence.

For CAIPIRINHA-VIBE, time-intensity plots demonstrated that moving images showed fluctuating signal intensities according to the vertical motion of the phantom (Fig. 3A, green line). Notably, after motion-correction, the variation in signal intensities decreased dramatically (Fig. 3A, red line). The CoV also decreased markedly from the moving (18.65) to the motion-corrected (2.56) image set. Indeed, the mean signal intensity and CoV of the motion-corrected images did not differ significantly from those of the static images ($p > 0.05$). These findings suggest that motion correction for aligning the subjects worked very well for CAIPIRINHA-VIBE by enhancing its motion insensitivity.

In radial-VIBE, the fluctuation of signal intensities on the time-intensity plots was similar in both non-motion-corrected and motion-corrected images; the mean signal intensities between the non-motion-corrected and motion-corrected images did not differ significantly ($p = 0.074$), which reflects that there was no significant motion in the phantom images due to the motion insensitivity of radial-VIBE. The CoV after motion correction (15.84) even increased, -compared to the images in moving mode (8.90), due to the non-rigid registration of streak artifacts ($p < 0.001$). These findings indicate that variations in signal intensity in non-motion-corrected and motion-corrected images mainly derived from motion-related streak artifacts rather than the movement of the subjects.

Regarding c-VIBE, the fluctuation of signal intensities on

Table 2. Effect of Breathing Motion to Signal Intensity, Noise and SNR of DCE-MRI Images

Parameter	Static	Moving	MOCO	*P* among Three Groups*	*P* between Two Groups†		
					Static vs. Moving	Moving vs. MOCO	MOCO vs. Static
Mean SI							
CAIPIRINHA-VIBE	690.33	600.50	716.08	< 0.001	< 0.001	< 0.001	0.058
Radial-VIBE	481.18	411.75	395.92	< 0.001	< 0.001	0.074	< 0.001
c-VIBE	660.56	575.85	580.44	< 0.001	< 0.001	> 0.999	< 0.001
SD							
CAIPIRINHA-VIBE	0.63	112.02	18.32	< 0.001	< 0.001	< 0.001	< 0.001
Radial-VIBE	0.15	36.63	62.71	< 0.001	< 0.001	< 0.001	< 0.001
c-VIBE	1.36	74.36	72.60	< 0.001	< 0.001	< 0.001	< 0.001
SNR							
CAIPIRINHA-VIBE	55.56	3.37	9.41	< 0.001	< 0.001	< 0.001	< 0.001
Radial-VIBE	48.81	4.3	4.96	< 0.001	< 0.001	< 0.001	< 0.001
c-VIBE	53.41	6.08	4.65	< 0.001	< 0.001	< 0.001	< 0.001
CoV (%)							
CAIPIRINHA-VIBE	0.09	18.65	2.56	< 0.001	< 0.001	< 0.001	0.054
Radial-VIBE	0.03	8.90	15.84	< 0.001	< 0.001	< 0.001	< 0.001
c-VIBE	0.21	12.91	12.50	< 0.001	< 0.001	0.153	< 0.001

*Analysis of variance was used to compare Mean SI, SD, and SNR between three groups, †Post-hoc *t* test with Bonferroni correction was used to compare Mean SI, SD, and SNR between two groups, and Levene's test was used to compare CoV between two groups.
c-VIBE = conventional VIBE, CAIPIRINHA = controlled aliasing in parallel imaging results in higher acceleration, CoV = coefficients of variation, DCE-MRI = dynamic contrast-enhanced-magnetic resonance imaging, MOCO = motion correction, SD = standard deviation, SI = signal intensity, SNR = signal-to-noise ratio, VIBE = volumetric interpolated breath-hold examination

time-intensity plots was similar in both moving and motion-corrected images. There were no significant differences in the mean signal intensities ($p > 0.999$) or the CoVs ($p = 0.153$) of the moving and motion-corrected images. These findings indicate that motion correction may not be helpful for improving the image quality of c-VIBE moving images.

Signal-to-Noise Ratio

The SNR according to motion mode within each sequence differed significantly by sequence ($p < 0.001$) (Table 2). Both CAIPIRINHA-VIBE (3.37 for the moving state and 9.41 for the motion-corrected state; $p < 0.001$) and radial-VIBE (4.3 for the moving state and 4.96 for the motion-corrected state; $p < 0.001$) had improved SNRs after motion correction. In c-VIBE, the SNR worsened with motion correction, which indicates that the overlapped motion-corrected images of the distorted phantom negatively affected the SNR.

DISCUSSION

In our phantom study, in terms of breathing motion artifacts and signal stability, the use of CAIPIRINHA-VIBE with motion correction might have been better than radial-VIBE and c-VIBE for free-breathing DCE-MRI. CAIPIRINHA, a recently developed PAT scheme, modifies the acquisition pattern by shifting the sampling positions (i.e., delta shift) from their normal positions in the partition-encoding direction. By using the extra delta shift, CAIPIRINHA can compensate for the inherent aliasing artifact caused by applying high acceleration factors (19).

We postulate that the motion-resistant characteristics of CAIPIRINHA-VIBE mainly rely on reducing the image distortion during motion due to its advanced PAT scheme in both the partition-encoding and frequency-encoding directions (6-8). The shape of the phantom tubes was maintained without after-images motion, so that motion correction could align the images of moving subjects as seen on the supplemental material and Figure 2A. In addition, the measured signal intensities of the moving subject in the motion-corrected images were similar to those of the static subject (Fig. 3A) and showed excellent stability (CoV, 2.56%) over 6 minutes. These characteristics enabled us to reliably use the measured signal intensities for pharmacokinetic analysis to calculate perfusion parameters.

MRI images using CAIPIRINHA-VIBE for the moving mode showed mildly distorted images due to PAT and in-folding artifacts. PAT artifacts are known to be related to higher in-plane spatial resolution and a higher acceleration factor. In a previous study, the PAT artifact did not significantly hamper the overall image quality of gadoxetic-acid-enhanced liver MRI (19). The ghosting of edges is also closely related to the order of the k-space sampling.

It is worth comparing the characteristics of CAIPIRINHA-VIBE with those of radial-VIBE and c-VIBE, which are both commonly used for DCE-MRI in the torso. Notably, on the moving mode acquired with radial-VIBE, there was no motion of the phantom in the images (Fig. 2B). These results support that radial-VIBE is motion-insensitive due to its radial k-space sampling scheme to acquire data in a spoke-wheel fashion (2, 12). However, radial-VIBE images were noisy and substantially degraded in the moving mode due to the streak artifacts that are characteristic of radial-VIBE due to under-sampling and/or susceptibility-related effects (12, 20, 21). Indeed, the SNR of radial-VIBE was inferior to that of CAIPIRINHA-VIBE (4.96 vs. 9.41 for motion-corrected images), and the signal stability of radial-VIBE in the moving state was also not good (CoVs, 8.9% with moving images and 15.84% with motion-corrected images).

In radial-VIBE with KWIC view-sharing, with the long temporal footprint, the acquisition time for a fully sampled image (i.e., full-frame image) might have been another source of image degradation in the moving mode (2, 22). With KWIC, the peripheral k-space of a sub-frame image shares data from neighboring subsets obtained at different time points, whereas the central k-space of each sub-frame image uses data acquired from a single timely subset (2, 21). Although KWIC was developed to increase the image quality of sub-frame images, unfortunately, breathing motion effects accumulated during the time to acquire a full-frame image may negatively influence the sub-frame images. In our study, we acquired a full-frame image for 30.6 seconds and generated six sub-frame images. Therefore, each sub-frame image could be influenced by breathing motion over 30.6 seconds rather than its frame time of 5.1 seconds. In contrast, CAIPIRINHA-VIBE and c-VIBE did not have this issue and were exposed to the breathing motion only for the acquisition time.

In terms of c-VIBE, it was originally developed to acquire 3D T1-weighted volumetric-interpolated images during a single breath-hold (7, 23). c-VIBE has been known to be sensitive to motion artifacts because it uses rectilinear

Korean Journal of Radiology
KJR

Cartesian k-space sampling. Our phantom study also demonstrated that c-VIBE was substantially degraded with both moving and motion-corrected images due to image blurring, distortion and after-images. In addition, the measured signal intensities in c-VIBE may not be reliable because overlapped after-images of the moving subject may mask the true variation in signal intensity along time points. Therefore, it may not be appropriate to use c-VIBE for free-breathing DCE-MRI.

Motion correction function is generally incorporated into commercial software used for analyzing DCE-MRI. However, motion correction is mainly used to align dynamic images to a reference image. In our study, we demonstrated that motion correction works efficiently when the objects move with preserved original shape, such as for CAIPIRINHA-VIBE. However, motion correction may not improve the distortion of subject images or artifacts, as demonstrated in the c-VIBE and radial-VIBE phantom images.

This study has a few limitations. The phantom used in this study obviously cannot completely represent the human body, and unexpected effects may have influenced MRI image quality. Similarly, the moving phantom platform is not identical to natural respiration movement in humans. For example, the liver does not move vertically in a straight line during true respiration (24); instead, liver movement is more complex, with cranio-caudal, lateral, and anterior-posterior motions (25, 26). In spite of these limitations, however, our study clearly visualized motion effects on each sequence and provided quantitative indices such as signal intensity, SD, SNR, and CoV during simulated breathing motions. Therefore, this preliminary phantom study may serve as a baseline study in establishing free-breathing DCE-MRI protocols.

In conclusion, our phantom study suggests that CAIPIRINHA-VIBE might be the best sequence for free-breathing DCE-MRI after motion correction, and it provides excellent image quality. Additional clinical studies should be undertaken to apply this result to real practice.

Supplementary Movie Legends

Movie 1. This video shows dynamic MRI images of the phantoms using CAIPIRINHA-VIBE, radial-VIBE, and c-VIBE in static, moving, and motion-corrected moving modes. The differences in breathing motion effects between three MRI sequences are clearly demonstrated in this video.

REFERENCES

1. Thng CH, Koh TS, Collins DJ, Koh DM. Perfusion magnetic resonance imaging of the liver. *World J Gastroenterol* 2010;16:1598-1609
2. Kim KW, Lee JM, Jeon YS, Kang SE, Baek JH, Han JK, et al. Free-breathing dynamic contrast-enhanced MRI of the abdomen and chest using a radial gradient echo sequence with k-space weighted image contrast (KWIC). *Eur Radiol* 2013;23:1352-1360
3. Kim B, Lee CK, Seo N, Lee SS, Kim JK, Choi Y, et al. Comparison of CAIPIRINHA-VIBE, Radial-VIBE, and conventional VIBE sequences for dynamic contrast-enhanced (DCE) MRI: a validation study using a DCE-MRI phantom. *Magn Reson Imaging* 2016;34:638-644
4. Hintze C, Stemmer A, Bock M, Kuder TA, Risse F, Dinkel J, et al. A hybrid breath hold and continued respiration-triggered technique for time-resolved 3D MRI perfusion studies in lung cancer. *Rofo* 2010;182:45-52
5. Breuer FA, Blaimer M, Mueller MF, Seiberlich N, Heidemann RM, Griswold MA, et al. Controlled aliasing in volumetric parallel imaging (2D CAIPIRINHA). *Magn Reson Med* 2006;55:549-556
6. McKenzie CA, Lim D, Ransil BJ, Morrin M, Pedrosa I, Yeh EN, et al. Shortening MR image acquisition time for volumetric interpolated breath-hold examination with a recently developed parallel imaging reconstruction technique: clinical feasibility. *Radiology* 2004;230:589-594
7. Vogt FM, Antoch G, Hunold P, Maderwald S, Ladd ME, Debatin JF, et al. Parallel acquisition techniques for accelerated volumetric interpolated breath-hold examination magnetic resonance imaging of the upper abdomen: assessment of image quality and lesion conspicuity. *J Magn Reson Imaging* 2005;21:376-382
8. AlObaidy M, Ramalho M, Busireddy KK, Liu B, Burke LM, Altun E, et al. High-resolution 3D-GRE imaging of the abdomen using controlled aliasing acceleration technique-a feasibility study. *Eur Radiol* 2015;25:3596-3605
9. Jackson E. Technical Committee MR Phantom Development/ Data Efforts. Web site. http://qibawiki.rsna.org/images/3/34/RSNA_QIBA_May2010_MR_Phantom.pdf. Accessed January 21, 2017
10. Lin W, Guo J, Rosen MA, Song HK. Respiratory motion-compensated radial dynamic contrast-enhanced (DCE)-MRI of chest and abdominal lesions. *Magn Reson Med* 2008;60:1135-1146
11. Chandarana H, Block TK, Rosenkrantz AB, Lim RP, Kim D, Mossa DJ, et al. Free-breathing radial 3D fat-suppressed T1-weighted gradient echo sequence: a viable alternative for contrast-enhanced liver imaging in patients unable to suspend respiration. *Invest Radiol* 2011;46:648-653
12. Song HK, Dougherty L. Dynamic MRI with projection reconstruction and KWIC processing for simultaneous high spatial and temporal resolution. *Magn Reson Med*

2004;52:815-824
13. Song HK, Dougherty L. k-space weighted image contrast (KWIC) for contrast manipulation in projection reconstruction MRI. *Magn Reson Med* 2000;44:825-832
14. Chefd'hotel C, Hermosillo G, Faugeras O. *Flows of diffeomorphisms for multimodal image registration*. In: *Proceedings of the IEEE International Symposium on Biomedical Imaging*. Piscataway, NJ: Institute of Electrical and Electronics Engineers, 2002:753-756
15. Reed GF, Lynn F, Meade BD. Use of coefficient of variation in assessing variability of quantitative assays. *Clin Diagn Lab Immunol* 2002;9:1235-1239
16. Dietrich O, Raya JG, Reeder SB, Reiser MF, Schoenberg SO. Measurement of signal-to-noise ratios in MR images: influence of multichannel coils, parallel imaging, and reconstruction filters. *J Magn Reson Imaging* 2007;26:375-385
17. Sodickson DK, Griswold MA, Jakob PM, Edelman RR, Manning WJ. Signal-to-noise ratio and signal-to-noise efficiency in SMASH imaging. *Magn Reson Med* 1999;41:1009-1022
18. Reeder SB, Wintersperger BJ, Dietrich O, Lanz T, Greiser A, Reiser MF, et al. Practical approaches to the evaluation of signal-to-noise ratio performance with parallel imaging: application with cardiac imaging and a 32-channel cardiac coil. *Magn Reson Med* 2005;54:748-754
19. Yu MH, Lee JM, Yoon JH, Kiefer B, Han JK, Choi BI. Clinical application of controlled aliasing in parallel imaging results in a higher acceleration (CAIPIRINHA)-volumetric interpolated breathhold (VIBE) sequence for gadoxetic acid-enhanced liver MR imaging. *J Magn Reson Imaging* 2013;38:1020-1026
20. Block KT, Uecker M, Frahm J. Undersampled radial MRI with multiple coils. Iterative image reconstruction using a total variation constraint. *Magn Reson Med* 2007;57:1086-1098
21. Fujinaga Y, Ohya A, Tokoro H, Yamada A, Ueda K, Ueda H, et al. Radial volumetric imaging breath-hold examination (VIBE) with k-space weighted image contrast (KWIC) for dynamic gadoxetic acid (Gd-EOB-DTPA)-enhanced MRI of the liver: advantages over Cartesian VIBE in the arterial phase. *Eur Radiol* 2014;24:1290-1299
22. Haider CR, Riederer SJ, Borisch EA, Glockner JF, Grimm RC, Hulshizer TC, et al. High temporal and spatial resolution 3D time-resolved contrast-enhanced magnetic resonance angiography of the hands and feet. *J Magn Reson Imaging* 2011;34:2-12
23. Kim BS, Lee KR, Goh MJ. New imaging strategies using a motion-resistant liver sequence in uncooperative patients. *Biomed Res Int* 2014;2014:142658
24. Clifford MA, Banovac F, Levy E, Cleary K. Assessment of hepatic motion secondary to respiration for computer assisted interventions. *Comput Aided Surg* 2002;7:291-299
25. Suramo I, Päivänsalo M, Myllylä V. Cranio-caudal movements of the liver, pancreas and kidneys in respiration. *Acta Radiol Diagn (Stockh)* 1984;25:129-131
26. Korin HW, Ehman RL, Riederer SJ, Felmlee JP, Grimm RC. Respiratory kinematics of the upper abdominal organs: a quantitative study. *Magn Reson Med* 1992;23:172-178